The Potential of COSMO-SkyMed SAR Images in Monitoring Snow Cover Characteristics

S. Pettinato, *Member, IEEE*, E. Santi, *Member, IEEE*, M. Brogioni, *Member, IEEE*, S. Paloscia, *Fellow, IEEE*, E. Palchetti, and Chuan Xiong

***Abstract*—Monitoring of snow cover is crucial to the study of global climate changes for water resource management, as well as for flood and avalanche risk prevention. The sensitivity to snow characteristics of X-band backscattering of COSMO-SkyMed mission has been analyzed in the framework of experimental and model activities. X-band data have been found to contribute to the retrieval of the snow water equivalent (SWE), provided that the snow cover is characterized by a snow depth (SD) of roughly 60–70 cm (SWE $>$ 100–150 mm) and with relatively large crystal dimensions. Subsequently, an algorithm for retrieving SD or SWE has been developed and tested with experimental data collected on several ground stations.**

***Index Terms*—COSMO-SkyMed, snow, snow depth (SD), snow water equivalent (SWE).**

I. Introduction

SNOW cover is the major component of the cryosphere and plays a significant role in the global water cycle and the climate system. Snow can be considered alternately as a resource and a threat. Abundant snowfalls are responsible for a great storage of water useful for hydroelectric purposes and water resource replenishment. However, sudden snow melting due to rapid increases in air temperature can also be responsible for dangerous flash floods and for avalanches. Production of snow cover maps is therefore very important in the study of global changes and in water resource management, as well as in flood and avalanche risk prevention.

Due to the increasing number and magnitude of natural disasters caused by global changes, the use of satellite data for a timely monitoring of the Earth's surface has become ever more appealing. Many national and international projects are aimed at contributing to protection from floods, avalanches, and landslides by developing a series of products derived from satellite sensors, which can be useful by allowing immediate assessment of the areas at risk and/or aid decision making on relief and cleanup operations. One Italian project, coordinated by the Italian Space Agency (ASI) and the Department of Civil Protection (DPC), was PROSA, which aimed at generating Earth observation products for meteorological alert against floods and landslides.

Manuscript received December 12, 2011; revised February 20, 2012; accepted February 25, 2012. Date of publication May 11, 2012; date of current version September 7, 2012. This work was supported in part by the Italian Space Agency (ASI), through the Constellation Of small Satellites for Mediterranean basin Observation-SkyMed 1720 HYDROCOSMO and PROSA projects, and in part by Regione Toscana in the frame of the CTOTUS project.

S. Pettinato, E. Santi, M. Brogioni, S. Paloscia, and E. Palchetti are with the Institute of Applied Physics of the National Research Council, Firenze, Italy (e-mail: s.paloscia@ifac.cnr.it).

C. Xiong is with the IFAC-CNR, Firenze, Italy, and also with the Institute for Remote Sensing Applications, Beijing 100101, China.

Color versions of one or more of the figures in this paper are available online at http://ieeexplore.ieee.org.

Digital Object Identifier 10.1109/LGRS.2012.2189752

Optical sensors have been proven capable of monitoring snow cover in cloud-free conditions, and several systems have been developed for operational monitoring of snow parameters from remote sensing data (e.g., [1]–[3]). However, only microwave sensors are able to acquire data independently of daylight and in adverse weather conditions. The potential of radar systems in mapping the extent of wet snow cover was investigated by using both airborne and satellite systems and was demonstrated in several works (e.g., [1]–[7]). Indeed, penetration of microwaves in the snowpack depends on electromagnetic frequency and on snow conditions; at the frequencies of currently available synthetic aperture radars (SARs) at C- and X-bands, penetration is high in dry snow and very low in wet snow [4], [10]. Thus, the estimation of the snow water equivalent (SWE) with the present available satellite SAR systems remains a challenge. Models and experiments have shown that C-band data are not suitable for separating dry snow from snow-free areas. However, wet snow can be detected by using a change detection approach because, in this case, the backscattering is of the order 2–3 dB lower than that of dry snow-covered soil [4], [11], [12].

Other studies have shown that, differently to wet snow, the effect of dry snow in Alpine regions on C-band backscattering is too small to detect snow cover and that a higher frequency is necessary for snow retrievals [10]. Research carried out in the framework of the Italian project PROSA has pointed out the possibility of generating snow cover maps by combining optical data from MODIS and ENVISAT SAR [10], [12].

Although the X-band is not yet the most suitable frequency for the retrieval of snow depth (SD) or SWE, some improvements are expected following the launch of the new X-band SAR systems (COSMO-SkyMed and TerraSAR-X). The aim of this letter is to evaluate the potential of these SAR sensors, and COSMO-SkyMed in particular, in providing information on snow characteristics in different physical conditions.

An experiment, described in the following sections, was set up on a test area in the Italian Alps by using a series of COSMO-SkyMed images, ground measurements of snow cover, and meteorological information.

II. COSMO-SkyMed Mission

COSMO-SkyMed (CSK) is a dual-use (civilian and defense) end-to-end Earth Observation System aimed at establishing a global service supplying provision of data, products, and services relevant to a wide range of applications, such as risk management, scientific and commercial applications, and defense applications [8]. The system consists of a constellation of four low-Earth-orbit midsize satellites, each equipped with a multimode high-resolution SAR operating at the X-band, with a sun-synchronous orbit at an $\sim$620-km height. The sensor operates in different observation modes. Following the launch of the last satellite in autumn 2010, all four radars are currently

in orbit to observe the Earth's surface in single or double polarization and in a relatively wide range of incident angles. These features allow the system a multiple-imaging opportunity over the same area in a very short time, with a full constellation revisit time of 12 h, although not with the same repeat pass geometry. It thus becomes possible to estimate land surface parameters through multiangle observations [13].

III. Sensitivity of X-Band Backscattering to Dry Snow

A. Experiment and Results

An experiment devoted to the analysis of the potentials of CSK images in snow characteristic monitoring took place in the eastern Italian Alps (Cordevole basin) and included meteorological and conventional snow measurements as well. The site was selected for a long-term snow monitoring experiment since 2002, combining continuous winter ground observations with microwave radiometers [15], [16], meteorological sensors, and satellite data. It is a relatively flat area located on the Mount Cherz (2010 m asl), which was particularly convenient for comparing snow and backscattering data (central coordinates: Lat 46.51 N and 11.87 E). A meteorological station located close to the area provided usual meteorological data and, in particular, air temperature.

A series of 20 COSMO-SkyMed images were collected between 2009 and 2011. The SAR images were fully calibrated by taking into account the real size of the scattering area in each pixel according to terrain slope. The ground resolution of CSK images used for this experiment ranged from 10 to 50 m. The local incidence angle (LIA) was obtained from a digital elevation model (DEM) and the knowledge of orbital and imaging parameters.

In addition to microwave data, all the significant parameters of snow cover (grain shape and size, snow density, water equivalent, volumetric liquid water content (LWC), temperature, and hardness) were measured with conventional approaches along vertical profiles in selected transects by the Avalanche Center in Arabba, simultaneously to the satellite overpasses. The measurement of LWC was carried out using standard methods [17]. Additional LWC measurements were occasionally carried out by using two electromagnetic probes: the Snow Fork (TOIKKA-Finland) and a probe built by IFAC-CNR.

As a first step, the cross-calibration of the images was checked by comparing the backscatter extracted over some reference targets (e.g., rock areas), which exhibited almost constant trends in the period of December 2010/January 2011. Furthermore, since the available images were acquired with different acquisition geometries, the backscattering coefficient was normalized for the LIA. Temporal trends of backscattering coefficient in VV polarization and SWE measurements collected in this location from August 2, 2010 to April 3, 2011 are represented in Fig. 1. The backscattering coefficient was averaged considering a homogeneous area (600 m by 700 m) on Mount Cherz (forests and possible layover/shadow effects were excluded). Table I lists the corresponding mean values of snow parameters (SD, snow density, SWE, and grain equivalent radius) measured on ground.

We can see from the diagram that the backscattering remains almost constant until the SWE of dry snow accumulated on soil is higher than 100–150 mm and increases rapidly as SWE rises to 400 mm. As snow starts melting (in late March), the backscattering decreases down to the level of bare soil, in spite of a further increase of SWE.

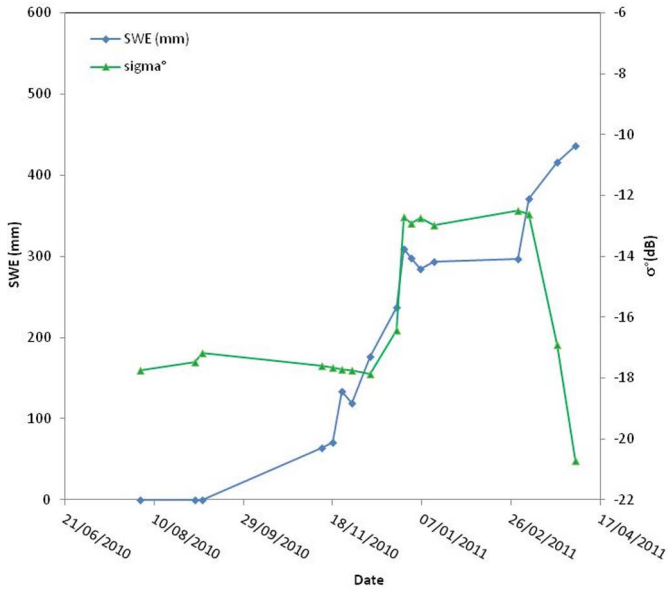

Fig. 1. (Green triangles) X-band backscattering coefficient at VV polarization and (blue rhombs) SWE measured on the Cherz plateau at 35° incidence angle as a function of time (in days).

TABLE I
Snow Depth, SD (in Centimeters), Snow Density, SWE, and Grain Equivalent Radius Measured on Ground for the Same Dates of the Diagram of Fig. 1

DATES	Snow depth (cm)	Density (kg/m3)	SWE (mm)	Equivalent Radius (mm)
06/12/2010	77.00	247.00	190.19	0.67
13/12/2010	62.00	264.00	163.68	0.65
16/12/2010	60.00	273.00	163.80	0.63
20/12/2010	63.00	261.00	164.43	0.62
27/12/2010	117.00	264.00	308.88	0.54
03/01/2011	106.00	270.00	286.20	0.34
10/01/2011	107.00	264.00	282.48	0.61
17/01/2011	106.00	288.00	305.28	0.55
24/01/2011	105.00	301.00	316.05	0.63
02/02/2011	107.00	279.00	298.53	0.77
07/02/2011	106.00	283.00	299.98	0.86
14/02/2011	105.00	291.00	305.55	0.91
21/02/2011	121.00	273.00	330.33	0.65
28/02/2011	132.00	274.00	361.68	0.91
07/03/2011	126.00	295.00	371.00	0.89
14/03/2011	129.00	254.00	328.00	0.68
21/03/2011	144.00	267.00	390.00	0.84
28/03/2011	137.00	323.00	442.00	1.00
05/04/2011	120.00	363.00	436.00	Wet snow
11/04/2011	90.00	403.00	360.00	Wet snow
18/04/2011	80.00	423.00	328.00	Wet snow
26/04/2011	51.00	412.00	206.00	Wet snow

B. Model Simulations

X-band backscattering sensitivity to dry snow at different polarizations and incidence angles was first exploited by means of a theoretical model, based on the coupling of the advanced integral equation method (AIEM) [18], [19] and the dense medium radiative transfer theory under the quasi-crystalline approximation (DMRT-QCA) [20]. The contribution of vegetation over soil was accounted for by using the so-called "cloud model" [21], in order to derive the total backscattering of the vegetated surface from the backscattering of bare surfaces, simulated by the AIEM. This combination of models was chosen due to its wide validity range and flexibility, while the DMRT-QCA was selected because it can account for a wide range of

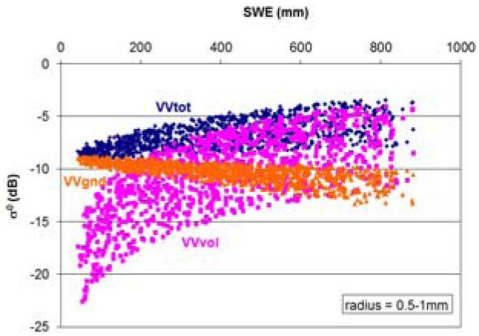

Fig. 2. Modeled X-band backscattering at $\theta = 25^\circ$ incidence angle as a function of SWE for a range of crystal radius between 0.5 and 1.0 mm (pink: contribution of the snow layer; orange: contribution of soil, computed with the Oh *et al.* semiempirical model [10]; and blue: total contribution). The spread of data is due to a parameterization of soil parameters (moisture and roughness) and snow density in a range of expected average values.

particle sizes and for the adhesive properties of the ice crystals. DMRT-QCA is a discrete model in which dry snow is modeled as a slab (or a stack of slab for the multilayer version) of random discrete spherical particles embedded in air upon a semi-infinite medium (the soil). The DMRT is able to describe the propagation and scattering in a dense medium (where the particles occupy an appreciable fractional volume, the particles can occupy more than 10% or up to 50% of the total volume) and also for the scattering of correlated scatterers (through the pair distribution function). The DMRT-QCA model used in this work is based on [20] and accounts for the full volume multiple scattering. This feature is important because it makes the simulation of the backscattering at cross-polarization possible [20]. In the present work, the snowpack was modeled as a single layer.

Several configurations of dry snowpack with different values of SWE, density, and scatterer dimension were tested. In particular, simulations have been carried out for SD ranging between 10 and 150 cm, snow density between 200 and 300 kg/m^3, grain radius between 0.1 and 1.0 mm, and incidence angle between 20° and 70°. Simulations showed that an appreciable sensitivity of X-band backscattering to dry snow can be found for SWE higher than 70–100 mm and relatively high values of snow density and crystal dimensions. As an example, in Fig. 2 the sensitivity of VV backscattering to SWE for a range of effective crystal radius between 0.5 and 1 mm is shown. No significant differences were found considering the HH and HV polarizations.

This model was validated by Tsang *et al.* [20] and subsequently verified on our test area, although with few experimental points available. The backscattering simulated by using DMRT was compared with the experimental values of backscattering measured over the Cherz plateau. The model was run considering a minimum SWE value > 100 mm and the ratio between SWE and the effective grain radius limited within an interval $(250\text{–}600 \cdot 10^3$ kg/m$^3)$ derived from the ground measurements. The regression equations between both simulated and measured backscattering and SWE, obtained for the two datasets are the following:

$$\sigma^{\circ}_{\mathrm{VV(model)}} = 8.8ln(\mathrm{SWE}) - 61.64 (R^2 = 0.47)$$
$$\sigma^{\circ}_{\mathrm{VV(exp)}} = 8.681ln(\mathrm{SWE}) - 62.7 (R^2 = 0.84).$$

The agreement between the two data sets is rather good, with very similar equations in terms of slopes.

The analysis of snow parameters during this period and the model simulations confirmed that the variations of SD, density, and grain size can be able to produce the sharp increase of backscattering up to 5 dB as noted in the experimental data represented in Fig. 1. The results obtained by the model simulations justified implementing an inversion algorithm for the retrieval of SWE from CSK images.

TABLE II
SAR DATA USED TO TEST THE ALGORITHM

Date	Sensor	Sensor Mode	Polarization
08/03/2009	CSK2	STR_HIMAGE	HH
27/05/2009	CSK2	STR_HIMAGE	HH
14/07/2009	CSK2	STR_HIMAGE	HH
22/01/2010	CSK2	STR_HIMAGE	HH
26/03/2010	CSK2	STR_PINGPONG	VV/VH
29/03/2010	CSK1	STR_PINGPONG	VV/VH
02/09/2010	CSK1	STR_PINGPONG	VV/VH

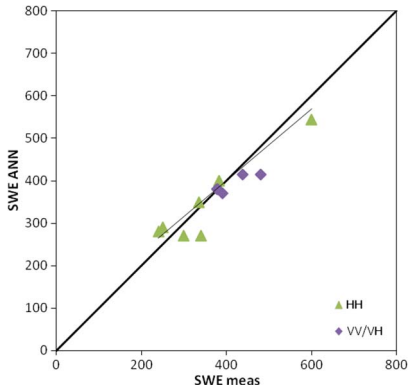

Fig. 3. SWE estimated by ANN compared with SWE measured on ground at the meteorological stations. The measured SWE was obtained from the five closest dconversion of SD through an average snow density of 250 kg/m^3. The regression equation is $\mathrm{SWE_{ANN}} = 0.844\ \mathrm{SWE_{meas}} + 62.4\ (R^2 = 0.82)$. Dates are some of those listed in Table I: March 8, 2009; January 22, 2010; and March 26 and 29, 2010.

IV. RETRIEVAL ALGORITHM

On the basis of these encouraging results, a subsequent effort was carried out for implementing a retrieval algorithm based on an artificial neural network (ANN) [22], [23]. Inputs to the ANN are the X-band backscattering measured in the available polarizations, the corresponding reference value measured in snow-free conditions, and the LIA obtained from the DEM of the area along with the orbital data. The output is the estimate of the SWE. The training of the ANN was performed by using data simulated with electromagnetic models (DMRT coupled with AIEM), while the reference values of snow-free soil were simulated using the AIEM only [18], [19]. The training set was generated by iterating the model simulations 10 000 times and by randomly varying the model inputs in a range derived from the direct measurements, thus obtaining a set of backscattering coefficients for each input vector of snow parameters. In this case, the training was carried out starting from values of SWE > 100 mm and limiting the ratio between SWE and the effective grain radius within the interval $250\text{–}600 \cdot 10^3$ kg/m^3. Two ANNs have been set up and trained separately considering as input the two polarizations VV/VH and the single polarization HH, respectively, according to the available CSK images. After completing the training, the ANNs were tested on a different data set (again of 10 000 samples), obtained by further iterating the procedure described earlier. The use of a pseudorandom function for generating the model inputs would have prevented a correlation between these two data sets.

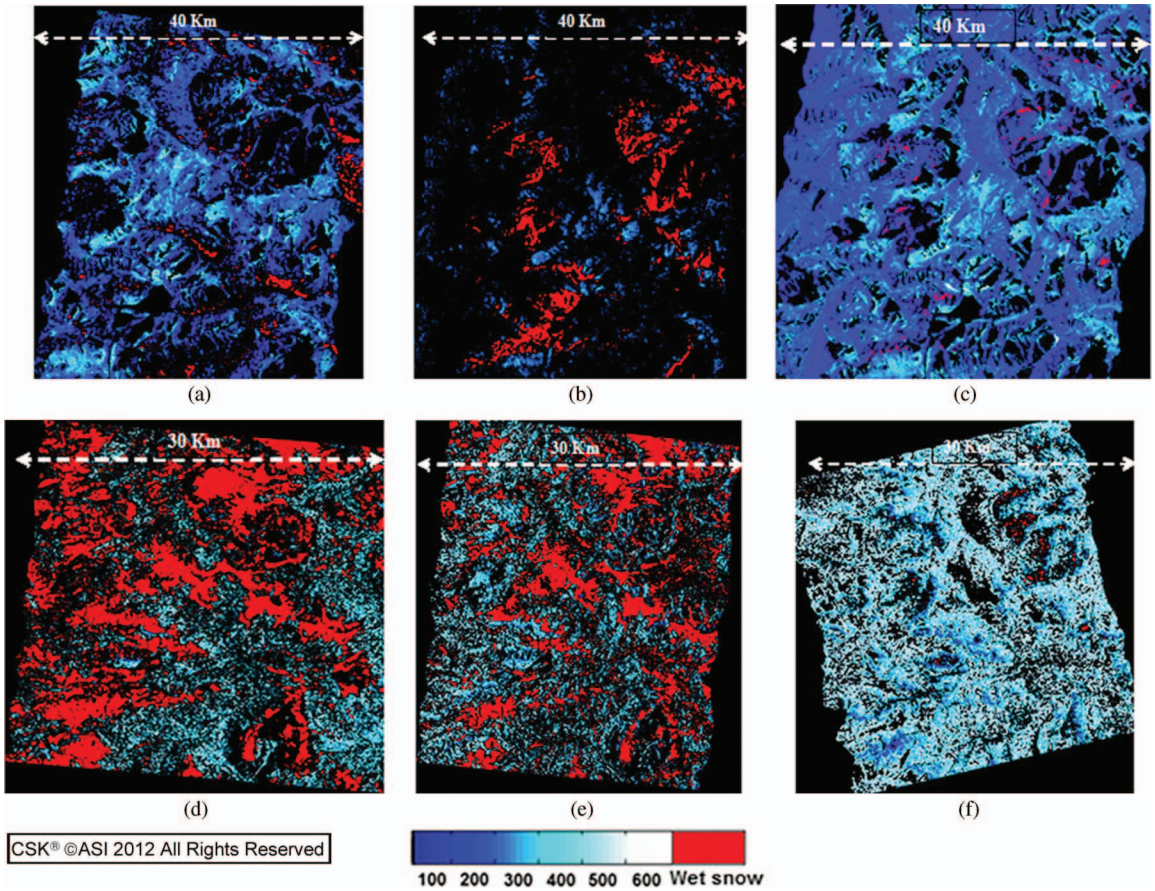

Fig. 4. SWE maps of the Cordevole test area generated from COSMO-SkyMed data. Red: Wet snow. From blue to white: Dry snow. Black: Masked areas. The scale of SWE starts from 100 mm. Dimensions of the images are 40 km × 40 km for Himages (HH polarization) and 30 km × 30 km for Ping Pong (VV–VH polarization). (a) 08-03-2009, obtained using the HH polarization. (b) 27-05-2009, obtained using the HH polarization. (c) 22-01-2010, obtained using the HH polarization. (d) 26-03-2010, obtained using the VV–VH polarization. (e) 29-03-2010, obtained using the VV–VH polarization. (f) 01-01-2011, obtained using the VV–VH polarization. Processing by IFAC-CNR, Courtesy of ASI, ©ASI 2012.

It was shown that, although the ANN inputs did not consider certain model parameters which were barely available (e.g., the important parameter of the average crystal dimension), the training process rapidly converged, and once the ANN architecture was optimized, the estimate of the output reached very good values. In particular, for a configuration with two hidden layers of 13 neurons each and an activating function of "tansig" type, assuming the availability of COSMO-SkyMed data in two polarizations (co- and cross-polar), the determination coefficient (R^2) was higher than 0.8, with an associated probability value (P-value) of 95%. The root-mean-square error was about 50 mm of water equivalent.

V. Test of the Algorithm With Experimental Data

The algorithm was then tested with experimental data collected on five subareas of the test site located close to five meteorological stations. The CSK images used for this comparison are listed in Table II.

It should be noted that, in these stations, snow was characterized by the SD, while the algorithm is calibrated in SWE. Therefore, in order to perform the comparison between the algorithm outputs and ground data, SD data were converted to SWE by assuming an average value of snow density of 250 kg/m^3 (considering that the measured snow density values range between 200 and 300 kg/m^3). Fig. 3 represents the comparison between SWE estimated by the ANN and SWE measured on ground (derived from the SD measured at the meteorological stations) obtained by using single polarization (HH) or dual co-cross polarization (VV/VH) X-band data as inputs to the algorithm, respectively. Points refer to different dates in winter 2009 and 2010 (March 8, 2009; January 22, 2010; and March 26 and 29, 2010). We can see that the regression line is close to 1 : 1 line and that the determination coefficient is rather high $(R^2 > 0.8)$. The results of the algorithm using HH polarization only or VV and HV polarizations are very similar.

VI. Generation of Snow Maps

Using the developed algorithm, snow cover maps were generated from COSMO-SkyMed data. In general, the algorithm allowed for the possibility of detecting the presence of wet snow and dry snow and, in case of dry snow, the estimate of some levels of SWE, provided that the latter had a value $\geq$ 100–150 mm.

The algorithm was applied to the areas which showed backscattering coefficients higher than the snow-free reference, assuming that the backscattering enhancement was due to snow characterized by a SWE $>$ 100–150 mm and therefore able to contribute to the radar response at the X-band. Since the choice of the snow-free image significantly affects the retrieval of wet snow, the snow-free reference was obtained by averaging the available CSK images collected in snow-free conditions in summer. On the remaining areas of the image, characterized by backscattering coefficients equal or lower than the snow-free

reference values, a further classification was carried out in order to separate wet snow from dry snow, undetectable at the X-band, and from snow-free surfaces. Wet snow, when present, was identified by using a threshold criterion derived from [5]. In the remaining areas, where backscattering was close to the snow-free reference values, dry snow with a SWE $<$ 100–150 mm was separated from the snow-free surfaces using ancillary information on air temperature and elevation, derived from the meteorological stations and from the DEM of the area, respectively.

As an example, Fig. 4(a)–(f) shows the SWE maps of the Cordevole test area generated from COSMO-SkyMed data for the following dates: 08-03-2009, 27-05-2009, 22-01-2010 (obtained from CSK Himages in HH polarizations), 26-03-2010, 29-03-2010, and 01-01-2011 (obtained from CSK Ping Pong in VV–VH polarizations). In these maps, the presence of wet snow was marked as red, whereas dry snow ranged from blue to white according to the SWE values. The estimate of SWE started from values $>$ 100 mm. The temporal evolution of snow cover was well pointed out in the map series. In January 2010 and 2011 [see Fig. 4(c) and (f)], almost all snow was dry, with very high SWE (particularly in January 2011). The snow melting started in March [see Fig. 4(a)] and became evident in the two maps at the end of March 2010 [dominance of red colors; see Fig. 4(d) and (e)]. At the end of May [see Fig. 4(b)], the snow extent was dramatically reduced, and most snow cover is wet.

These results, although not validated on a large scale, have been confirmed even by the meteorological information collected on the area (SD and air temperature at different levels collected at the nine meteorological stations present in the area and by the punctual ground measurements. The "reliability" index of the maps of Fig. 4, which accounts for the percentage of bad input data and the estimate of output parameters outside the established range (outliers), is generally higher than 0.8.

VII. Summary and Future Work

The sensitivity of ASI/COSMO-SkyMed X-band SAR to snow cover and SWE has been investigated by using experimental results and model simulations. An algorithm for generating snow cover maps and estimating SWE has been developed and tested with experimental data. The test was carried out on an alpine area in Northern Italy where previous experiments on snow monitoring had been performed by using microwave and *in situ* sensors.

X-band data have been found to contribute to the retrieval of SWE for SD greater than about 60–70 cm (SWE $>$ 100–150 mm) and relatively high crystal size. Although a clear validation of the snow maps obtained with this method was missing, the temporal series of maps showed a good agreement with the meteorological information, the seasonal evolution of snow cover, and the available ground truth.

This result is encouraging, although more investigations and data validations are necessary to demonstrate the full potential of COSMO-SkyMed SAR in snow detection, particularly in areas characterized by high snowfall accumulation, such as the Alps in Europe and the Rocky Mountains in the U.S.

Acknowledgment

The authors would like to thank A. Crepaz and A. Cagnati of the Avalanche Center in Arabba (BL, Italy) for their kind assistance in gathering and interpreting snow data on the Cherz area.

References

[1] K. D. Hall, G. A. Riggs, V. V. Salomonson, N. E. DiGirolamo, and K. J. Bayr, "MODIS snow-cover products," *Remote Sens. Environ.*, no. 83, pp. 181–194, Jan. 2002.

[2] K. D. Hall, J. L. Foster, D. L. Verbyla, A. G. Klein, and C. S. Benson, "Assessment of snow-cover mapping accuracy in a variety of vegetation-cover densities in Central Alaska," *Remote Sens. Environ.*, vol. 66, no. 2, pp. 129–137, Nov. 1998.

[3] V. V. Salomonson and I. Appel, "Development of the Aqua MODIS NDSI fractional snow cover algorithm and validation results," *IEEE Trans. Geosci. Remote Sens.*, vol. 44, no. 7, pp. 1747–1756, Jul. 2006.

[4] T. Nagler and H. Rott, "Retrieval of wet snow by means of multitemporal SAR data," *IEEE Trans. Geosci. Remote Sens.*, vol. 38, no. 2, pp. 754–765, Mar. 2000.

[5] J. Shi and J. Dozier, "Estimation of snow water equivalence using SIR-C/X-SAR. I. Inferring snow density and subsurface properties," *IEEE Trans. Geosci. Remote Sens.*, vol. 38, no. 6, pp. 2465–2474, Nov. 2000.

[6] T. Guneriussen, H. Johnsen, and I. Lauknes, "Snow cover mapping capabilities using RADARSAT standard mode data," *Can. Remote. Sens.*, vol. 27, no. 2, pp. 109–117, 2001.

[7] S. Pettinato, E. Malnes, and J. Haarpaintner, "Snow cover maps with satellite borne SAR: A new approach in harmony with fractional optical SCA retrieval algorithms," in *Proc. IEEE IGARSS*, 2006, pp. 726–729.

[8] K. P. Luojus, J. T. Pulliainen, S. J. Metsamaki, and M. T. Hallikainen, "Snow-covered area estimation using satellite radar wide-swath images," *IEEE Trans. Geosci. Remote Sens.*, vol. 45, no. 4, pp. 978–989, Apr. 2007.

[9] J. T. Koskinen, J. T. Pulliainen, K. P. Luojus, and M. Takala, "Monitoring of snow-cover properties during the spring melting period in forested areas," *IEEE Trans. Geosci. Remote Sens.*, vol. 48, no. 1, pp. 50–58, Jan. 2010.

[10] S. Pettinato, E. Santi, M. Brogioni, S. Paloscia, and P. Pampaloni, "An operational algorithm for snow cover mapping in hydrological applications," in *Proc. IEEE IGARSS*, 2009, vol. 4, pp. IV-964–IV-967.

[11] Y. Oh, K. Sarabandi, and F. T. Ulaby, "An empirical model and an inversion technique for radar scattering from bare soil surfaces," *IEEE Trans. Geosci. Remote Sens.*, vol. 30, no. 2, pp. 370–381, Mar. 1992.

[12] S. Pettinato, E. Santi, M. Brogioni, G. Macelloni, S. Paloscia, and P. Pampaloni, "An operational algorithm for snow cover mapping by using optical and SAR data," in *Proc. ESA SP*, Bergen, Sweden, Jun. 28–Jul. 2, 2010.

[13] F. Covello, F. Battazza, A. Coletta, G. Manoni, and G. Valentini, "COSMO-SkyMed mission status: Three out of four satellites in orbit," in *Proc. IEEE IGARSS*, 2009, vol. 2, pp. II-773–II-776.

[14] A. Cagnati, A. Crepaz, G. Macelloni, P. Pampaloni, R. Ranzi, M. Tedesco, M. Tomirotti, and M. Valt, "Study of the snow melting—Refreezing cycle using multi-sensor data and snow modelling," *J. Glaciol.*, vol. 50, no. 170, pp. 419–426, 2004.

[15] G. Macelloni, S. Paloscia, P. Pampaloni, M. Brogioni, R. Ranzi, and A. Crepaz, "Monitoring of melting refreezing cycles of snow with microwave radiometers: The Microwave Alpine Snow Melting Experiment (MASMEx 2002–2003)," *IEEE Trans. Geosci. Remote Sens.*, vol. 43, no. 11, pp. 2431–2442, Nov. 2005.

[16] M. Brogioni, G. Macelloni, E. Palchetti, S. Paloscia, P. Pampaloni, S. Pettinato, E. Santi, A. Cagnati, and A. Crepaz, "Monitoring snow characteristics with ground-based multifrequency microwave radiometry," *IEEE Trans. Geosci. Remote Sens.*, vol. 47, no. 11, pp. 3643–3655, Nov. 2009.

[17] S. C. Colbeck, E. Akitaya, R. Armstrong, H. Gubler, J. Lafeuille, K. Lied, D. McClung, and E. Morris, "International classification for seasonal snow on the ground," in *Proc. Int. Comm. Snow Ice-IAHS*, 1990.

[18] K. S. Chen, T. D. Wu, L. Tsang, Q. Li, J. Shi, and A. K. Fung, "Emission of rough surfaces calculated by the integral equation method with comparison to three-dimensional moment method simulations," *IEEE Trans. Geosci. Remote Sens.*, vol. 41, no. 1, pp. 90–101, Jan. 2003.

[19] T. D. Wu and K. S. Chen, "A reappraisal of the validity of the IEM model for backscattering from rough surfaces," *IEEE Trans. Geosci. Remote Sens.*, vol. 42, no. 4, pp. 743–753, Apr. 2004.

[20] L. Tsang, J. Pan, D. Liang, Z. Li, D. W. Cline, and Y. Tan, "Modeling active microwave remote sensing of snow using dense media radiative transfer (DMRT) theory with multiple-scattering effects," *IEEE Trans. Geosci. Remote Sens.*, vol. 45, no. 4, pp. 990–1004, Apr. 2007.

[21] E. P. W. Attema and F. T. Ulaby, "Vegetation modeled as a water cloud," *Radio Sci.*, vol. 13, no. 2, pp. 357–364, 1978.

[22] K. Hornik, "Multilayer feed forward networks are universal approximators," *Neural Netw.*, vol. 2, no. 5, pp. 359–366, 1989.

[23] A. Linden and J. Kinderman, "Inversion of multilayer nets," in *Proc. Int. Joint Conf. Neural Netw.*, 1989, vol. II, pp. 425–430.